Crystal Structure of *Methanococcus voltae* RadA in Complex with ADP: Hydrolysis-Induced Conformational Change†

Xinguo Qian, Yan Wu, Yujiong He, and Yu Luo*

Department of Biochemistry, University of Saskatchewan, A3 Health Sciences Building, 107 Wiggins Road, Saskatoon, Saskatchewan, Canada S7N 5E5

Received June 24, 2005; Revised Manuscript Received August 11, 2005

ABSTRACT: Members of a superfamily of RecA-like recombinases facilitate a central strand exchange reaction in the DNA repair process. Archaeal RadA and Rad51 and eukaryal Rad51 and meiosis-specific DMC1 form a closely related group of recombinases distinct from bacterial RecA. Nevertheless, all such recombinases share a conserved core domain which carries the ATPase site and putative DNA-binding sites. Here we present the crystal structure of an archaeal RadA from *Methanococcus voltae* (MvRadA) in complex with ADP and Mg^{2+} at 2.1 Å resolution. The crystallized RadA−ADP filament has an extended helical pitch similar to those of previously determined structures in the presence of nonhydrolyzable ATP analogue AMP-PNP. Structural comparison reveals two recurrent conformations with an extensive allosteric effect spanning the ATPase site and the putative DNA-binding L2 region. Varied conformations of the L2 region also imply a dynamic nature of recombinase-bound DNA.

Homologous strand exchange promoted by RecA-like recombinases enables repair of double-stranded DNA breaks and restart of stalled replication forks (*1*−*5*) by using a homologous DNA strand as the template in a diploid or replicating cell. This recombinase superfamily (*6*) is composed of bacterial RecA (*7*), archaeal RadA or Rad51 (*8*), and eukaryal Rad51 (*9*) and meiosis-specific DMC1 (*10*). In *Escherichia coli*, a double-stranded break is first processed by unwinding and asymmetric exonuclease digestion to produce a long stretch of single-stranded DNA (ssDNA)[1] (*11*−*13*). In the presence of ATP and Mg^{2+}, the recombinase first coats this primary ssDNA to form a nucleoprotein filament often termed the presynaptic complex, which has ATPase and strand exchange activities (*14*). The presynaptic complex pools double-stranded DNA (dsDNA) and aligns it with the ssDNA to form the synaptic complex. DNA strand exchange ensues to form a heteroduplex DNA (hdDNA) between the ssDNA and its complementary strand in the dsDNA substrate, while the like strand in the dsDNA substrate is displaced from the nucleoprotein filament (*5*, *15*, *16*). The substrates and products of this reaction can be conveniently separated and quantified on agarose gels.

Despite large differences at the amino acid sequence level (*17*), all known RecA-like recombinases share a conserved design that consists of an ATPase domain preceded by a short β-stranded polymerization motif (*18*, *19*). Documented microscopic and crystallographic results have revealed a common tale of two right-handed helical structures: an extended "active" form and a compact "inactive" form (*20*−*27*). Recently, yeast Rad51 and MvRadA have been crystallized in the extended filamentous form (*28*, *29*). In both structures, the ATPase sites were placed between protomers, a feature reminiscent of the electron microscopy-reconstructed active filament of *E. coli* RecA (EcRecA) (*30*). The ATPase domain also carries putative DNA-binding loops L1 and L2 located near the filament axis (*24*). ATP hydrolysis is required for filament disassembly at the 5′ end of ssDNA (*31*, *32*). The conservation of a functional ATPase site implies an essential role by ATP hydrolysis in DNA strand exchange. The interplay between ATP hydrolysis and strand exchange, however, is less understood. ATP hydrolysis appears to be advantageous for extensive strand exchange promoted by EcRecA (*33*−*36*) and by human DMC1 (*37*), while conditions in the absence of ATP hydrolysis have been found for extensive strand exchange reactions promoted by human and yeast Rad51 proteins (*38*, *39*). It is worth noting that a time-resolved fluorescence study has demonstrated ATP hydrolysis-related flexibility in EcRecA-bound DNA (*40*), which may be advantageous for achieving optimal alignment between sequence repeats due to a putative motorlike activity of EcRecA (*40*). At least one other motor model is being entertained to explain EcRecA's ability to bypass heterologous insertions in DNA substrates (*15*, *32*). For decades, EcRecA has been the most studied protein in this superfamily. Our crystallographic study of MvRadA appears to indicate that the archaeal recombinase is a more feasible structural prototype. To visualize the structural consequences of ATP hydrolysis, we determined the crystal structure of MvRadA in complex with ADP and Mg^{2+}. Comparison with the available MvRadA structures revealed two recurrent conformations of the DNA-binding L2 region,

† This work is supported by SHRF Establishment Grant 1425, NSERC Discovery Grant 161981-03, and CIHR Operating Grant 63860. Y.L. is a recipient of a CIHR New Investigator Salary Award.

* To whom correspondence should be addressed. Telephone: (306) 966-4379. Fax: (306) 966-4390. E-mail: yu.luo@usask.ca.

[1] Abbreviations: MvRadA, RadA recombinase from *Methanococcus voltae*; EcRecA, RecA recombinase from *E. coli*; AMP, adenosine 5′-monophosphate; ATP-γ-S, adenosine 5′-*O*-(3-thiotriphosphate); ssDNA, single-stranded DNA; dsDNA, double-stranded DNA; hdDNA, heteroduplex DNA; AMP-PNP, 5′-adenylyl imidodiphosphate.

10.1021/bi051222i CCC: $30.25
Published on Web 10/01/2005

Table 1: X-ray Crystallographic Data[a] and Structure Refinement Statistics

crystallographic data			
PDB entry	1Z4D	1Z4C	1Z4B
description	AMP-PNP, 0.6 M KAc	AMP-PNP, 0.3 M KAc	ADP, 0.5 M KCl
unit cell dimensions (Å)	$a = b = 83.7$, $c = 105.4$	$a = b = 83.5$, $c = 106.8$	$a = b = 84.0$, $c = 106.4$
resolution range[b] (Å)	2.0 (2.1−2.0)	2.3 (2.4−2.3)	2.1 (2.2−2.1)
no. of observed reflections	158268	60009	105032
no. of unique reflections	28217	17245	24905
completeness (%)[b]	99.8 (99.1)	91.2 (89.5)	99.3 (99.1)
R_{sym}[b,c]	0.039 (0.279)	0.046 (0.244)	0.042 (0.340)
I/σ	14.9/2.0	13.2/2.5	12.8/1.9
anomalous I/σ[b]	6.3 (3.4)	5.4 (3.8)	5.8 (2.4)
crystal structure refinement			
no. of reflections with $F > 0$	25544 (90.3%)	15494 (82.7%)	22875 (92.1%)
R-factor/R_{free}[d]	0.221/0.238	0.202/0.251	0.234/0.265
no. of residues, nucleotide	311, 1 AMP-PNP	299, 1 AMP-PNP	299, 1 ADP
no. of solvent molecules	100 waters and 5 ions	115 waters and 5 ions	64 waters and 3 ions
rsmd			
bonds (Å)	0.0062	0.0066	0.0065
angles (deg)	1.20	1.23	1.22
Ramachandran plot (%)			
most favored	91.9	90.5	92.0
disallowed	0	0	0

[a] Cu Kα radiation, wavelength of 1.5418 Å, space group $P6_1$. [b] Values in parentheses refer to values in the highest-resolution shell. [c] $R_{sym} = \sum|I_h - \langle I\rangle_h|/\sum I_h$, where $\langle I\rangle_h$ is average over symmetry equivalents and h is the reflection index. [d] R-factor $= \sum|F_{obs} - F_{calc}|/\sum F_{obs}$. R_{free} is calculated using a randomly selected 5% of the reflections set aside throughout the refinement.

which appear to be induced by structural changes at the ATPase site. Consistent with the fluorescence study (*40*), the flexibility of DNA in the ADP complex is implied by the disordered L2 loop.

EXPERIMENTAL PROCEDURES

Protein Preparation and Crystallization. RadA from *Methanococcus voltae* was subcloned into pET28a, overexpressed in BL21(DE3)-Codon+RIL cells (Stratagene), and purified as reported previously (*29*). In brief, the purification procedure involved steps of polymin P precipitation, high-salt extraction, and heparin affinity chromatography. The concentrated protein (~30 mg/mL) was crystallized using the hanging drop crystallization method at a room temperature of 21 °C. The optimal well solution for the crystallization of MvRadA−MgAMP-PNP complexes contained 2 mM AMP-PNP, 0.05 M $MgCl_2$, 0.6 or 0.3 M KAc, 6% PEG 3350, and 0.05 M Hepes-KOH buffer at pH 7.4. The optimal condition for MvRadA−MgADP crystals was similar to that of the MvRadA−AMP-PNP crystals, except for the use of ADP and 0.5 M KCl. All three types of crystals grew to a similar size of 0.2 mm × 0.2 mm × 0.4 mm in 3−7 days. ADP, AMP-PNP, and PEG 3350 were purchased from Sigma-Aldrich. The other chemicals were from VWR.

Data Collection and Structure Determination. Several crystals of each complex were gradually transferred to stabilization solutions composed of the well solution supplemented with 5, 10, 15, 20, and 25% glycerol, and then flash-cooled to 100 K in a nitrogen stream generated by an Oxford CryoSystem device. The 0.4° oscillation images of each crystal were acquired and processed using a Bruker Proteum-R system as described previously (*29*). The previously determined MvRadA models [Protein Data Bank (PDB) entries 1T4G and 1XU4] were used as the starting models for rigid body refinement. Each model was iteratively rebuilt using XtalView (*41*) and refined using CNS (*42*). A 2.8 Å resolution anomalous difference map was generated using model phases retarded by 90°. Ordered potassium sites were located at major peaks (>7σ) in the anomalous difference maps, while most minor peaks (3−5σ) corresponded to sulfur atoms. Statistics of the diffraction data from the most diffractive crystal of each type of the three complexes, refinement, and geometry are given in Table 1. To remove model bias, the omit $F_o - F_c$ map in Figure 2 was generated after simulated annealing from 1000 K. The molecular figures were generated using Molscript (*43*) and Raster3D (*44*). The coordinates and structure factors have been deposited in the PDB (entries 1Z4D, 1Z4C, and 1Z4B).

Strand Exchange Assay. The DNA substrates were chosen from a published study (*45*). Three oligonucleotides (#1, 63 nucleotides, ACAGCACCAG ATTCAGCAAT TAAGCTCTAA GCCATCCGCA AAAATGACCT CTTATCAAAA GGA; #45, 31 nucleotides, ACAGCACCAG ATTCAGCAAT TAAGCTCTAA G; and #55, 31 nucleotides, CTTAGAGCTT AATTGCTGAA TCTGGTGCTG T) were obtained from Intergrated DNA Technologies. Equal molarities of complementary oligonucleotides #45 and #55 were heated at 95 °C for 5 min and then slowly cooled to generate the dsDNA substrate. The solution for strand exchange reaction was composed of 3 mM ATP or an analogous nucleotide, 10 mM $MgCl_2$, 100 mM KCl or NaCl, 50 mM Hepes-Tris buffer at pH 7.2, and 10 μM MvRadA and 1 μM oligonucleotides. The 63-nucleotide ssDNA substrate (oligonucleotide #1) was preincubated at 37 °C with mvRadA for 1 min before addition of the dsDNA substrate. The reaction was stopped at 30 min by adding EDTA to a final concentration of 20 mM and trypsin to a final concentration of 1 μg/μL. After trypsin digestion for 10 min, a 10 μL sample was mixed with 5 μL of a loading buffer composed of 30% glycerol and 0.1% bromophenol blue, and then loaded onto a 17.5% acrylamide gel. The SDS−PAGE gel was developed, stained with ethidium bromide, and visualized with an UV illuminator. An optional ATP regeneration system was used as specified, which was composed of 6 mM phosphoenolpyruvate and 0.01 unit of pyruvate kinase/μL (New England Biolabs).

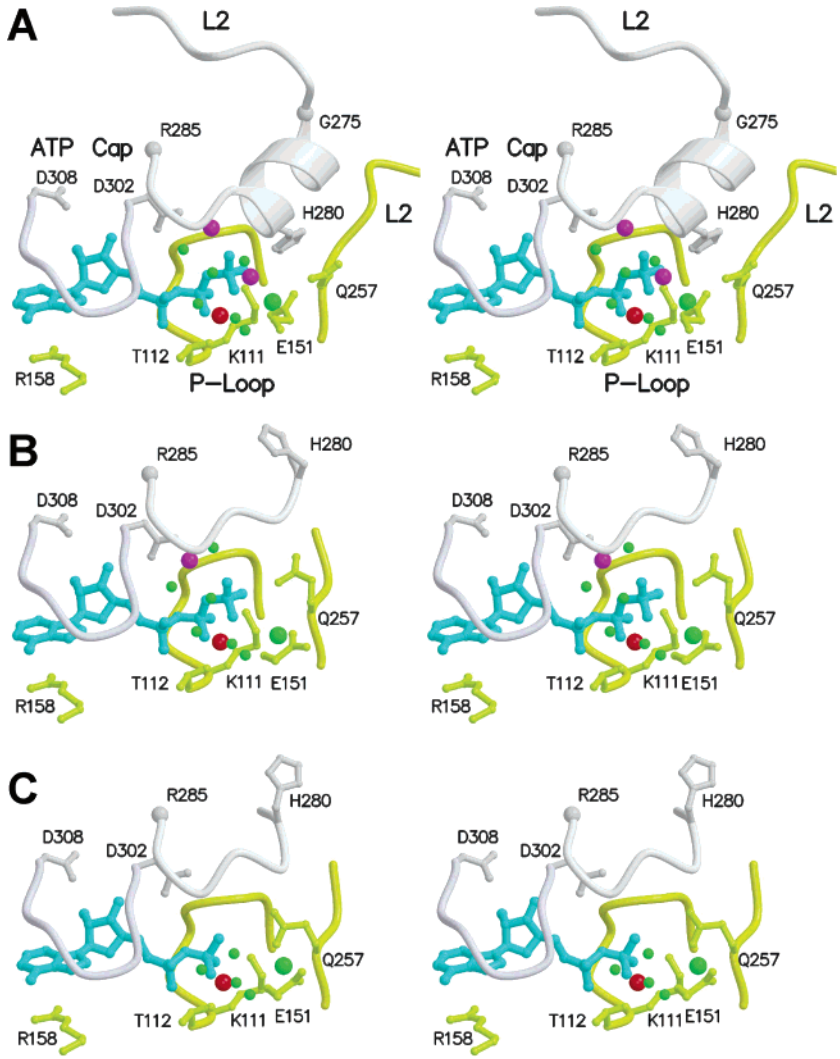

FIGURE 1: ATPase site of RadA in stereo. Two MvRadA subunits are colored yellow and gray. K^+ ions, Mg^{2+} ions, and water molecules are colored purple, red, and green, respectively. The putative hydrolysis water is shown as a larger sphere. (A) MvRadA complex in the presence of AMP-PNP and a high concentration of KAc. (B) MvRadA complex in the presence of AMP-PNP and a low concentration of KAc. (C) MvRadA complex in the presence of ADP. More residues in the L2 region are ordered in panel A, but similarly disordered in panels B and C.

RESULTS

Refined Structure of an ATPase-Active Conformation of RadA. High concentrations of certain inorganic salts have been observed as efficient substitutes for ssDNA in stimulating the ATPase activities of EcRecA and human Rad51 (*46*−*48*). For MvRadA, KCl has been identified as the substitute for ssDNA, and the ATPase-active filament has been determined at a resolution of 2.4 Å (*49*). The soaking experiment employed to convert the crystallized filaments into the ATPase-active form, however, had slightly compromised the diffractive power of the crystals. The resulting resolution was not adequate for locating solvent molecules in the proximity of the heavier triphosphate moiety and potassium ions. We therefore optimized the crystallization condition in the presence of 0.6 M KAc (high KAc, Table 1), which was observed to stimulate maximal ATPase activity (data not shown). The resolution was improved to 2.0 Å, which enabled us to make a detailed comparison with the other MvRadA structures (discussed below).

Crystals described in this study were grown under similar conditions. The crystals belong to space group $P6_1$ with similar helical pitches and essentially identical packing scheme (Table 1). The filament pitch coinciding with the crystallographic *c*-axis is 105.4 Å in the ATPase-active form. AMP-PNP, the nonhydrolyzable ATP analogue, is buried between MvRadA protomers (Figure 1A). One subunit (yellow subunit, Figure 1A) binds the ATP analogue and an octahedral Mg^{2+} largely through its conserved P-loop (residues Gly-105−Thr-112) (*50*) and the base-stacking Arg-158. The adjacent subunit (gray subunit, Figure 1A) contributes a region we denote the ATP cap (residues Asp-302−Asp-308) and the C-terminal portion of the L2 region. The putative ssDNA-binding L2 region (residues Asn-256−Arg-285) has an eight-residue helix (residues Gly-275−Ala-282) analogous to helix G of EcRecA (*24*). The His-280 side chain therein forms a direct hydrogen bond with the γ-phosphate of the ATP analogue. Two K^+ ions (purple spheres, Figure 1A) located by anomalous signals form bridges between the γ-phosphate and the backbone carbonyl moieties at the C-terminus of the eight-residue helix. Besides, one of the K^+ ions contacts the side chain of Asp-302, while the other contacts the side chain of Glu-151. A candidate for the hydrolyzing water is hydrogen bonded with the side chains of Glu-151 and Gln-257 from the subunit contributing the

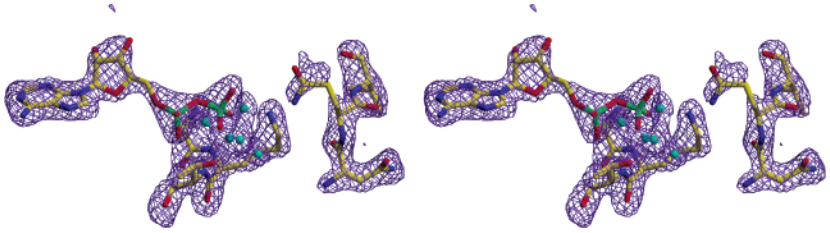

FIGURE 2: Electron density map at the ADP-binding site in stereo. The refined model of the ADP, P loop residues Gly-110−Thr-112, L2 elbow of Gln-257−Ser-259, and the magnesium site are shown. A 2.1 Å resolution omit difference electron density map is contoured at 3.0σ (purple). The orientation is identical to that of Figure 1C.

P-loop. The electron density contour for Gln-257 was well-defined. The analogous residues of EcRecA (Glu-96 and Gln-194) have been proposed as the catalytic residues on the basis of the EcRecA crystal structure (*24*) and analogy to GTPases (*51*). As expected for P-loop-containing ATPases and GTPases, the γ-phosphate contacts the ϵ-amino group of Lys-111 and the Mg^{2+} ion. With the added electron-withdrawing effects of His-280 and the two K^+ ions, the γ-phosphate is likely further polarized for the nucleophilic attack by the hydrolysis water positioned and activated by Glu-151 and Gln-257. The potassium−oxygen distances in the MvRadA structure fall between 2.6 and 2.9 Å, resembling the values revealed in the high-resolution structure of a potassium channel−Fab complex (*52*). The higher resolution also enabled us to locate more solvent molecules, including those forming the remnant hydration shell of the potassium ions. Despite the higher resolution, there was no interpretable electron density for residues Pro-262−Met-268. This L2 segment was previously modeled with high *B* factors in the KCl-soaked crystal (PDB entry 1XU4).

The RadA Complex with AMP-PNP at a Low Concentration of Potassium. The second type of MvRadA−AMP-PNP crystals was grown in the presence of 0.3 M KAc. The structure was refined to 2.3 Å resolution. The helical filament pitch of this form is 106.8 Å. The ATP analogue was located at an essentially identical position (Figure 2B) as observed in the ATPase-active form. Surprisingly, only one potassium ion was located by anomalous signals in the vicinity of the γ-phosphate. Candidates for three water ligands for the K^+ ion were also identified in the electron density map. In comparison, only two water ligands were identified for its counterpart in the ATPase-active form. Possibly due to the higher degree of hydration, this potassium ion was found farther (3.5 Å) from the γ-phosphate. As such, the γ-phosphate may not be adequately polarized for hydrolysis. Besides, the entire L2 region did not exhibit any regular secondary structure. There were no electron densities for a long stretch of residues from Ala-260 to Val-278. Notably, His-280 was located far from the ATP analogue. The catalytic side chains of Glu-151 and Gln-257 were found in different conformations. The electron density for the tip of the Gln-257 side chain was not well defined. On the other hand, electron densities for the main chain did not indicate the existence of alternate conformations. Our recent study has demonstrated that MvRadA's ATPase activity is sigmoidal with respect to both potassium and magnesium concentrations (*49*), suggesting some degree of cooperativity in forming active filaments. It is therefore not surprising that we observed abrupt rather than gradual structural changes after application of different doses of KAc.

RadA−ADP Complex. The MvRadA−ADP complex was refined to 2.1 Å resolution. The helical filament pitch of this form is 106.4 Å. ADP was located at a position (Figure 1C) essentially identical to those of its counterparts in the two AMP-PNP complexes. Compared with those of the MvRadA−AMP-PNP complexes, the diphosphate-binding P-loop did not show any apparent conformational change. There were no strong anomalous signals to indicate the presence of a potassium ion in the vicinity of the diphosphate moiety of ADP. Compared with that in the MvRadA−AMP-PNP complexes, the magnesium ion has one more water ligand located at the binding site for γ-phosphate. The ordered parts of the L2 region and the catalytic side chains of Glu-151 and Gln-257 are strikingly similar to their counterparts seen in the MvRadA−AMP-PNP crystals grown with a smaller dose of KAc (Figure 1B,C). The electron density for the side chain of Gln-257 was also weak (Figure 2). It is also worth noting that Gln-257 is located at the N-terminal elbow of the L2 region. Subtle conformational changes of this residue, as well as dramatic changes in the C-terminal elbow (around His-280) of the L2 region, may constitute an essential part of the allosteric effect on ATP hydrolysis.

Strand Exchange Promoted by RadA. In the presence of potassium, MvRadA was observed to promote a strand exchange reaction between a 63-nucleotide ssDNA and a 31 bp dsDNA. A significant amount of the reaction product, a 63-nucleotide/31-nucleotide hdDNA, was detected in the presence of ATP, ATP-γ-S, and AMP-PNP, but not in the absence of an ATP analogue or in the presence of ADP (Figure 3A). The nucleoside triphosphate-dependent strand exchange activity of MvRadA is consistent with known cofactor requirement for RecA-like recombinases.

The RadA H280N Mutant Is Inactive. The ATPase site of MvRadA is well-ordered in the presence of AMP-PNP and an activating dose of KAc as a mimic for DNA. The γ-phosphate is involved in a hydrogen bond network bridging Gln-257 and His-280 at either end of the DNA-binding L2 region. Besides, the planar γ-amide group of Gln-257 stacks against the imidazole ring of His-280 (Figure 1A). Both residues, especially His-280, were observed in distinct conformations as well as dispositions in the three reported crystal structures. The precise position of a catalytic Gln is well-known for its role in GTPase activation (*53*, *54*). The conserved Gln-194 of EcRecA has been found to be intolerant of mutations (*54*) and important for allosteric regulation (*51*). Counterparts of His-280 are invariable in archaeal and eukaryal homologues and somewhat conserved as a Phe in bacterial RecA proteins (Phe-217 in EcRecA). The Phe residue has been found to be somewhat tolerant of Tyr and Cys mutations but not of other amino acids (*55*).

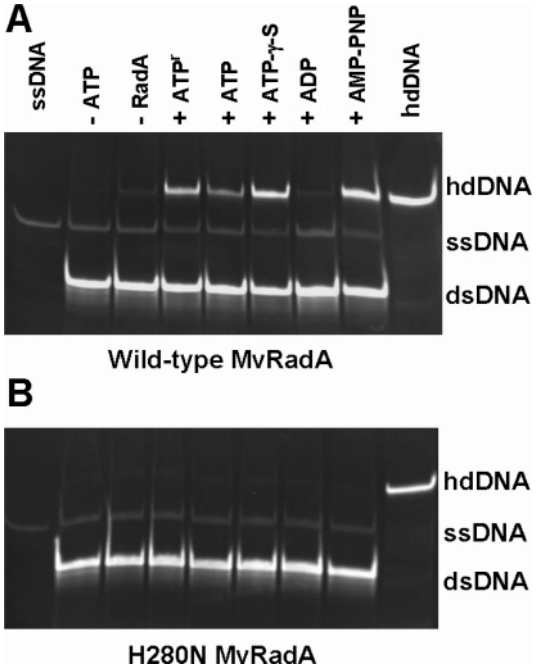

FIGURE 3: Strand exchange promoted by RadA. The reaction solution contained 100 mM KCl, 10 mM $MgCl_2$, 50 mM Hepes Tris buffer at pH 7.2, 3 mM nucleotide, 10 μM MvRadA, and a 63-nucleotide ssDNA and a 31 bp dsDNA (1 μM each). After incubation for 30 min at 37 °C, samples of the reaction mixture were removed, deproteinated, and separated by SDS−PAGE on a 17.5% acrylamide gel. The gel was stained by ethidium bromide. Strand exchange activity was detected by the formation of a 31-nucleotide−63-nucleotide heteroduplex DNA (hdDNA). (A) Strand exchange promoted by wild-type MvRadA. Activity is observed in the presence of ATP or its nonhydrolyzable analogues ATP-γ-S and AMP-PNP. (B) Lack of strand exchange activity of the MvRadA H280N protein. ATP^r denotes the use of an ATP regeneration system.

Interestingly, work on the F217Y mutant of EcRecA has suggested a regulatory role of this residue in transferring allosteric information across the subunit interface (*56*). Conceivably, a bulky phenyl ring at a similar disposition, though unable to form a hydrogen bond with the γ-phosphate, would also restrict and thus optimally place the conserved Gln for catalysis. In the MvRadA structures determined in the absence of either AMP-PNP or an adequately high concentration of a potassium salt, His-280 was found in a strikingly different location (Figure 1B,C). Concomitantly, electron densities for the γ-amide group of Gln-257 were weak, indicating some degree of structural disorder. In contrast to compact and extended types of MvRadA filaments with varied pitches and periodicities seen by electron microscopy (E. Egelman, personal communication), all the crystals reported here are essentially isomorphous. The largely unchanged crystal packing scheme apparently limited the periodicity to six protomers per turn and the extended pitches to a narrow range. The first seven N-terminal residues and five residues around Glu-164 are the only parts involved in crystal packing between MvRadA filaments. A differential influence of crystal packing on the ATPase site and DNA-binding loops is unlikely. We therefore argue that the lack of hydrogen bond links between the phosphate moiety and residues Gln-257 and His-280 seen in the MvRadA−ADP complex partly reveals the cross-talk between the ATPase site and the DNA binding site, and is a direct structural consequence of ATP hydrolysis. An Ala mutant at His-280's analogous position of yeast Rad51 has been found to be defective in binding DNA (*28*). We made a more conservative H280N MvRadA mutant. The purified mutant protein was soluble at a concentration of 1 mM and formed microcrystals. Misfolding is ruled unlikely. However, this mutant protein exhibited neither detectable ATPase (data not shown) nor strand exchange activity (Figure 3B). Possibly, stringent precision is required for the catalytic Gln and its partner His to promote ATP hydrolysis as well as strand exchange.

DISCUSSION

Two disordered loops, L1 and L2, in the first crystal structure of EcRecA were initially suggested as the DNA-binding site (*24*). The importance of the two loops has been further highlighted by studies on peptide mimics of L2 (*54*, *57*, *58*), mutagenesis (*59*−*61*), and chemical cross-linking with DNA (*60*, *62*−*64*). The entire L1 region (Arg-218−Arg-230) and the majority of the L2 region (Asn-256−Arg-285) are ordered in the ATPase-active form of MvRadA. This conformation appears to be recurrent in the MvRadA−AMP-PNP crystals either grown or soaked in activating concentrations of potassium salts. In comparison with the previously determined structure in the absence of a monovalent salt (PDB entry 1T4G), soaking in a high concentration of sodium salts did not produce any noticeable change (data not shown). The L2 region is largely disordered in the MvRadA−ADP crystal, despite being grown in high concentrations of KCl. The more ordered L2 conformation appears to be dependent on the presence of both the nonhydrolyzable ATP analogue and the high concentration of potassium salts. Since ADP cannot be utilized as a cofactor by RecA-like recombinases to promote DNA strand exchange, the disposition of the L1 and L2 regions seen only in the ATPase-active form may resemble an essential conformation in the strand exchange reaction. Adjacent L1 regions and L2 regions each form a continuous helical ridge along the filament axis (Figure 4A). The groove between the ridges harbors a high concentration of cationic residues (Arg-218, Arg-224, Arg-230, and Lys-261, colored cyan). The universally conserved Gly-274 and Gly-275 residues, which are located at the N-terminus of the helix G counterpart, are also positioned in this groove (Figure 4B). Both Gly residues of EcRecA have been found to be intolerant of mutations (*59*). The electrostatic nature of this groove appears to favor the binding of a polyanionic DNA substrate. Mutations at the analogous position of Arg-224 in homologues from two hyperthermophiles have been shown to be strand exchange-defective, indicating this site is important for interacting with DNA (*19*). Interestingly, Arg-224 is located in the proximity of the filament axis (Figure 4B). The relatively ordered nature of the ATPase-active form also implies that the DNA bound before ATP hydrolysis is relatively inflexible, consistent with the fluorescence study on EcRecA−DNA filament with ATP hydrolysis "poisoned" by ATP-γ-S (*40*).

All MvRadA structures have been determined in the extended filaments with similar helical pitches. The previously reported MvRadA−AMP-PNP complex determined in the absence of potassium (*29*) and the complex determined in an under-dose of potassium are similar as well as puzzling. The protomer arrangement in these extended MvRadA

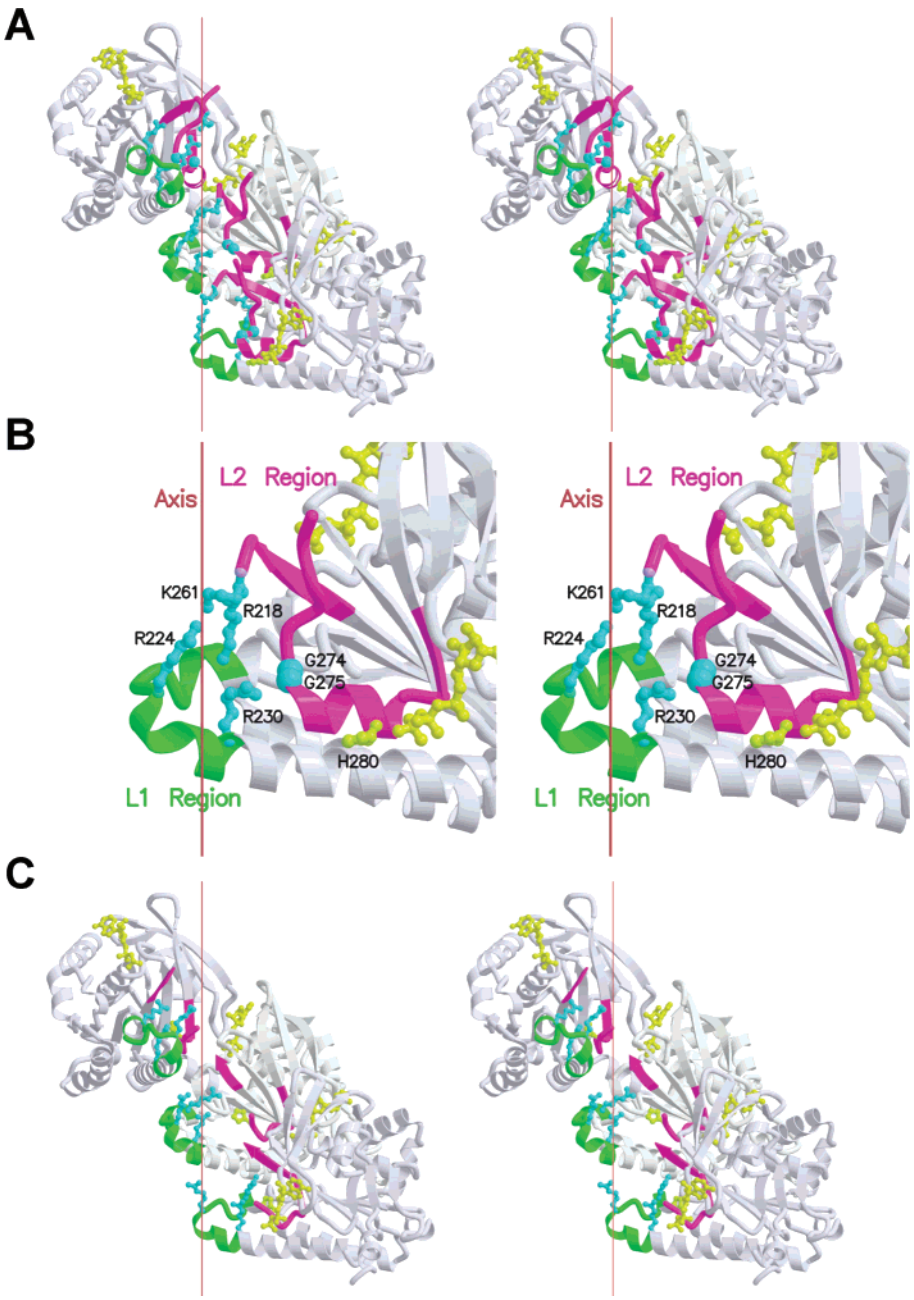

FIGURE 4: Putative ssDNA binding site in stereo. AMP-PNP and selected side chains are shown as a ball-and-stick model. The L1 and L2 regions are highlighted in green and magenta, respectively. The helical axis lies vertically. The AMP-PNP molecules and His-280 side chains are colored yellow. (A) Three adjacent ATPase core domains in the ATPase-active form. The putative DNA-binding groove between adjacent L1 and L2 regions is rich in cationic side chains. (B) L1 and L2 regions of one ATPase core domain in the ATPase-active form. Gly-274, Gly-275, Arg-218, Arg-224, Arg-230, Lys-261, and His-280 are colored cyan and labeled. (C) Three adjacent ATPase core domains in the MvRadA−ADP complex. A large portion of L2 is disordered.

filaments appears to resemble the electron microscopy-revealed feature in active EcRecA filaments (*30*). However, their ATPase sites apparently lack the precision for efficient ATP hydrolysis. The determination of the MvRadA−ADP complex in an essentially identical conformation argues that there is a second conformation within the extended filament complex as a result of ATP hydrolysis. Crystallization trials in the absence of nucleotide cofactors or in the presence of AMP never produced any crystal. The crystal packing interactions seem to be insufficient for enriching extended MvRadA filaments. As such, the extended MvRadA−ADP filaments, though surprising, may be somewhat stable in solution. Compared with the ATPase-active form, concerted conformational changes were located across the ATPase site and the DNA-binding L2 region. A large portion of the L2 region, which includes the two invariable Gly residues and the helix G counterpart, becomes disordered (Figure 4C). Conceivably, the putative DNA-binding groove would cease to exist. As a likely result, the affinity for DNA would decrease. The affinity decrease is consistent with findings that ATP hydrolysis is required for RecA and Rad51 dissociation from nucleoprotein filaments (*31*, *65*). Dissociation of a recombinase protomer requires the cleavage of protein−DNA and protein−protein interfaces. Removing a terminal protomer cleaves one protein−protein interface, while removing an internal protomer cleaves two. Even in the presence of ADP, the protomer interface appears to be somewhat stabilized with an essentially unchanged disposi-

tion of nucleotide-interacting P loop and Arg-158 of one protomer, and ATP cap of another. Conceivably, a decrease in protein−DNA affinity would result in dissociation at the filament end with minimal energetic cost. The crystal structures, however, do not provide an explanation for the observed 5′−3′ polarity. The largely disordered L2 region seen in the MvRadA−ADP crystal also implies that the recombinase-bound DNA is flexible, which is consistent with the time-resolved fluorescence study on EcRecA-bound DNA (*40*). Previous studies have suggested that EcRecA dissociates from the 5′ end of ssDNA (*31*, *32*), while protomer exchange is minimal within the presynaptic complex prior to strand exchange (*66*). On the other hand, a fluorescence study has demonstrated that the compact ATPase-inactive EcRecA filament cannot be directly converted into the extended active filament (*67*). For EcRecA and MvRadA with relatively fast ATP hydrolysis rates (10−30 min^{-1}), the presynaptic complex would survive several cycles of ATP hydrolysis and ADP−ATP exchange either in the absence of a homologous dsDNA or before the strand exchange reaction occurs. This possibility is consistent with kinetic findings on EcRecA, which exhibits much faster ATP hydrolysis than protomer exchange (*68*−*71*). During these multiple hydrolysis cycles, it is unlikely that the presynaptic complex would disassemble and reassemble, which would require protomer exchange. Conversion into the compact inactive filament is also unlikely, which would also require reassembling of the active filament since the reverse conversion from the resultant compact filament is prohibited. It is, therefore, consistent with the existing evidence that the presynaptic complex may remain in its extended form prior to strand exchange. Thus, we argue, sections of the recombinase-bound ssDNA may indeed be cycled through two conformational states in concert with ATP hydrolysis and nucleotide exchange. The conformational change or flexibility triggered by ATP hydrolysis may serve as a useful rationale in further studying the interplay between the ATPase site and the DNA-binding site(s). Most evidence for nucleotide exchange by active recombinase−DNA filaments, however, is implicit. Soaking MvRadA crystals in the absence of any nucleotide abolished the diffraction in 30 min followed by crystal dissolution in 2−3 h. The crystallized recombinase filaments seem to be somewhat dynamic to allow for loss of nucleotide cofactors sequestered between protomers. We then attempted ADP−AMP-PNP exchange by crystal soaking without success. It is worth noting most eukaryotic RecA orthologs are much slower ATPases than EcRecA. During ATP hydrolysis in the presence of a ATP regeneration system, human DMC1−ssDNA filaments accumulate much less ADP than human Rad51, despite being 2-fold faster in ATP hydrolysis (*72*, *73*). These results imply that DMC1 is faster in nucleotide exchange. Interestingly, human XRCC2 protein has recently been observed to stimulate ADP−ATP exchange by the slower human Rad51 (*74*).

In addition, similar conformational changes can alternatively be triggered within the extended MvRadA filament by the loss of either the K^+ ion(s) or the terminal phosphate of ATP. For human and yeast Rad51 proteins, but not for EcRecA, optimal conditions were found for extended strand exchange in the absence of ATP hydrolysis. The sequences of eukaryal homologues are more than 40% identical with that of MvRadA. They may share some aspects of structural plasticity visualized in the MvRadA structures in various doses of potassium acetate. We speculate that the dynamic nature of Rad51-bound DNA could be alternatively achieved *in vitro* by optimizing the reaction condition. The remotely related EcRecA, on the other hand, does not appear to require any monovalent cations for function. As such, RecA may not alter its grip on DNA unless the ATP cofactor is hydrolyzed.

RecA-like recombinases are well-known for their structural plasticity in forming helical filaments with remarkably heterogeneous ranges of helical pitches and periodicities. MvRadA filaments with extended helical pitches have been crystallized. Strikingly, the high-resolution structures revealed recurrent long-range conformational changes correlated with either K^+ loss or ATP hydrolysis. The conformational changes imply two conformations of the recombinase-bound DNA which differ in flexibility. This structural finding may provide a useful rationale for understanding the role of ATP hydrolysis in promoting the hallmark strand exchange reaction.

ACKNOWLEDGMENT

We thank the Saskatchewan Structural Sciences Centre for access to its X-ray facility.

REFERENCES

1. Cox, M. M. (1998) A broadening view of recombinational DNA repair in bacteria, *Genes Cells 3*, 65−78.
2. Cox, M. M., Goodman, M. F., Kreuzer, K. N., Sherratt, D. J., Sandler, S. J., and Marians, K. J. (2000) The importance of repairing stalled replication forks, *Nature 404*, 37−41.
3. Courcelle, J., Ganesan, A. K., and Hanawalt, P. C. (2001) Therefore, what are recombination proteins there for? *BioEssays 23*, 463−70.
4. Lusetti, S. L., and Cox, M. M. (2002) The bacterial RecA protein and the recombinational DNA repair of stalled replication forks, *Annu. Rev. Biochem. 71*, 71−100.
5. Kowalczykowski, S. C. (2000) Initiation of genetic recombination and recombination-dependent replication, *Trends Biochem. Sci. 25*, 156−65.
6. Seitz, E. M., and Kowalczykowski, S. C. (2000) The DNA binding and pairing preferences of the archaeal RadA protein demonstrate a universal characteristic of DNA strand exchange proteins, *Mol. Microbiol. 37*, 555−60.
7. Clark, A. J., and Margulies, A. D. (1965) Isolation and Characterization of Recombination-Deficient Mutants of Escherichia Coli K12, *Proc. Natl. Acad. Sci. U.S.A. 53*, 451−9.
8. Sandler, S. J., Satin, L. H., Samra, H. S., and Clark, A. J. (1996) recA-like genes from three archaean species with putative protein products similar to Rad51 and Dmc1 proteins of the yeast *Saccharomyces cerevisiae*, *Nucleic Acids Res. 24*, 2125−32.
9. Shinohara, A., Ogawa, H., and Ogawa, T. (1992) Rad51 protein involved in repair and recombination in *S. cerevisiae* is a RecA-like protein, *Cell 69*, 457−70.
10. Bishop, D. K., Park, D., Xu, L., and Kleckner, N. (1992) DMC1: A meiosis-specific yeast homolog of *E. coli* recA required for recombination, synaptonemal complex formation, and cell cycle progression, *Cell 69*, 439−56.
11. Dillingham, M. S., Spies, M., and Kowalczykowski, S. C. (2003) RecBCD enzyme is a bipolar DNA helicase, *Nature 423*, 893−7.
12. Taylor, A. F., and Smith, G. R. (2003) RecBCD enzyme is a DNA helicase with fast and slow motors of opposite polarity, *Nature 423*, 889−93.
13. Singleton, M. R., Dillingham, M. S., Gaudier, M., Kowalczykowski, S. C., and Wigley, D. B. (2004) Crystal structure of RecBCD enzyme reveals a machine for processing DNA breaks, *Nature 432*, 187−93.

14. Bianco, P. R., Tracy, R. B., and Kowalczykowski, S. C. (1998) DNA strand exchange proteins: A biochemical and physical comparison, *Front. Biosci. 3*, D570−603.
15. Cox, M. M. (2003) The bacterial RecA protein as a motor protein, *Annu. Rev. Microbiol. 57*, 551−77.
16. Kowalczykowski, S. C., Dixon, D. A., Eggleston, A. K., Lauder, S. D., and Rehrauer, W. M. (1994) Biochemistry of homologous recombination in *Escherichia coli*, *Microbiol. Rev. 58*, 401−65.
17. Brendel, V., Brocchieri, L., Sandler, S. J., Clark, A. J., and Karlin, S. (1997) Evolutionary comparisons of RecA-like proteins across all major kingdoms of living organisms, *J. Mol. Evol. 44*, 528−41.
18. Pellegrini, L., Yu, D. S., Lo, T., Anand, S., Lee, M., Blundell, T. L., and Venkitaraman, A. R. (2002) Insights into DNA recombination from the structure of a RAD51−BRCA2 complex, *Nature 420*, 287−93.
19. Shin, D. S., Pellegrini, L., Daniels, D. S., Yelent, B., Craig, L., Bates, D., Yu, D. S., Shivji, M. K., Hitomi, C., Arvai, A. S., Volkmann, N., Tsuruta, H., Blundell, T. L., Venkitaraman, A. R., and Tainer, J. A. (2003) Full-length archaeal Rad51 structure and mutants: Mechanisms for RAD51 assembly and control by BRCA2, *EMBO J. 22*, 4566−76.
20. Ogawa, T., Yu, X., Shinohara, A., and Egelman, E. H. (1993) Similarity of the yeast RAD51 filament to the bacterial RecA filament, *Science 259*, 1896−9.
21. Yang, S., VanLoock, M. S., Yu, X., and Egelman, E. H. (2001) Comparison of bacteriophage T4 UvsX and human Rad51 filaments suggests that RecA-like polymers may have evolved independently, *J. Mol. Biol. 312*, 999−1009.
22. Yang, S., Yu, X., Seitz, E. M., Kowalczykowski, S. C., and Egelman, E. H. (2001) Archaeal RadA protein binds DNA as both helical filaments and octameric rings, *J. Mol. Biol. 314*, 1077−85.
23. Yu, X., Jacobs, S. A., West, S. C., Ogawa, T., and Egelman, E. H. (2001) Domain structure and dynamics in the helical filaments formed by RecA and Rad51 on DNA, *Proc. Natl. Acad. Sci. U.S.A. 98*, 8419−24.
24. Story, R. M., Weber, I. T., and Steitz, T. A. (1992) The structure of the *E. coli* recA protein monomer and polymer, *Nature 355*, 318−25.
25. Datta, S., Prabu, M. M., Vaze, M. B., Ganesh, N., Chandra, N. R., Muniyappa, K., and Vijayan, M. (2000) Crystal structures of *Mycobacterium tuberculosis* RecA and its complex with ADP-AlF_4: Implications for decreased ATPase activity and molecular aggregation, *Nucleic Acids Res. 28*, 4964−73.
26. Datta, S., Krishna, R., Ganesh, N., Chandra, N. R., Muniyappa, K., and Vijayan, M. (2003) Crystal structures of *Mycobacterium smegmatis* RecA and its nucleotide complexes, *J. Bacteriol. 185*, 4280−4.
27. Rajan, R., and Bell, C. E. (2004) Crystal structure of RecA from *Deinococcus radiodurans*: Insights into the structural basis of extreme radioresistance, *J. Mol. Biol. 344*, 951−63.
28. Conway, A. B., Lynch, T. W., Zhang, Y., Fortin, G. S., Fung, C. W., Symington, L. S., and Rice, P. A. (2004) Crystal structure of a Rad51 filament, *Nat. Struct. Mol. Biol. 11*, 791−6.
29. Wu, Y., He, Y., Moya, I. A., Qian, X., and Luo, Y. (2004) Crystal Structure of Archaeal Recombinase RadA: A Snapshot of Its Extended Conformation, *Mol. Cell 15*, 423−35.
30. VanLoock, M. S., Yu, X., Yang, S., Lai, A. L., Low, C., Campbell, M. J., and Egelman, E. H. (2003) ATP-mediated conformational changes in the RecA filament, *Structure 11*, 187−96.
31. Shan, Q., Bork, J. M., Webb, B. L., Inman, R. B., and Cox, M. M. (1997) RecA protein filaments: End-dependent dissociation from ssDNA and stabilization by RecO and RecR proteins, *J. Mol. Biol. 265*, 519−40.
32. Cox, J. M., Tsodikov, O. V., and Cox, M. M. (2005) Organized unidirectional waves of ATP hydrolysis within a RecA filament, *PLoS Biol. 3*, e52.
33. Cox, M. M. (1994) Why does RecA protein hydrolyse ATP?, *Trends Biochem. Sci. 19*, 217−22.
34. Jain, S. K., Cox, M. M., and Inman, R. B. (1994) On the role of ATP hydrolysis in RecA protein-mediated DNA strand exchange. III. Unidirectional branch migration and extensive hybrid DNA formation, *J. Biol. Chem. 269*, 20653−61.
35. Shan, Q., Cox, M. M., and Inman, R. B. (1996) DNA strand exchange promoted by RecA K72R. Two reaction phases with different Mg^{2+} requirements, *J. Biol. Chem. 271*, 5712−24.
36. Bedale, W. A., and Cox, M. (1996) Evidence for the coupling of ATP hydrolysis to the final (extension) phase of RecA protein-mediated DNA strand exchange, *J. Biol. Chem. 271*, 5725−32.
37. Sehorn, M. G., Sigurdsson, S., Bussen, W., Unger, V. M., and Sung, P. (2004) Human meiotic recombinase Dmc1 promotes ATP-dependent homologous DNA strand exchange, *Nature 429*, 433−7.
38. Morrison, C., Shinohara, A., Sonoda, E., Yamaguchi-Iwai, Y., Takata, M., Weichselbaum, R. R., and Takeda, S. (1999) The essential functions of human Rad51 are independent of ATP hydrolysis, *Mol. Cell. Biol. 19*, 6891−7.
39. Sung, P., and Stratton, S. A. (1996) Yeast Rad51 recombinase mediates polar DNA strand exchange in the absence of ATP hydrolysis, *J. Biol. Chem. 271*, 27983−6.
40. Ramreddy, T., Sen, S., Rao, B. J., and Krishnamoorthy, G. (2003) DNA dynamics in RecA-DNA filaments: ATP hydrolysis-related flexibility in DNA, *Biochemistry 42*, 12085−94.
41. McRee, D. E. (1999) XtalView/Xfit: A versatile program for manipulating atomic coordinates and electron density, *J. Struct. Biol. 125*, 156−65.
42. Brunger, A. T., Adams, P. D., Clore, G. M., DeLano, W. L., Gros, P., Grosse-Kunstleve, R. W., Jiang, J. S., Kuszewski, J., Nilges, M., Pannu, N. S., Read, R. J., Rice, L. M., Simonson, T., and Warren, G. L. (1998) Crystallography & NMR system: A new software suite for macromolecular structure determination, *Acta Crystallogr. D54* (Part 5), 905−21.
43. Kraulis, P. (1991) MOLSCRIPT: A program to produce both detailed and schematic plots of protein structures, *J. Appl. Crystallogr. 24*, 946−50.
44. Bacon, D. J., and Anderson, W. F. (1988) A Fast Algorithm for Rendering Space-Filling Molecule Pictures', *J. Mol. Graphics 6*, 219−20.
45. Mazin, A. V., Zaitseva, E., Sung, P., and Kowalczykowski, S. C. (2000) Tailed duplex DNA is the preferred substrate for Rad51 protein-mediated homologous pairing, *EMBO J. 19*, 1148−56.
46. Pugh, B. F., and Cox, M. M. (1988) High salt activation of recA protein ATPase in the absence of DNA, *J. Biol. Chem. 263*, 76−83.
47. Tombline, G., and Fishel, R. (2002) Biochemical characterization of the human RAD51 protein. I. ATP hydrolysis, *J. Biol. Chem. 277*, 14417−25.
48. Liu, Y., Stasiak, A. Z., Masson, J. Y., McIlwraith, M. J., Stasiak, A., and West, S. C. (2004) Conformational changes modulate the activity of human RAD51 protein, *J. Mol. Biol. 337*, 817−27.
49. Wu, Y., Qian, X., He, Y., Moya, I. A., and Luo, Y. (2005) Crystal structure of an ATPase-active form of Rad51 homolog from *Methanococcus voltae*. Insights into potassium dependence, *J. Biol. Chem. 280*, 722−8.
50. Saraste, M., Sibbald, P. R., and Wittinghofer, A. (1990) The P-loop: A common motif in ATP- and GTP-binding proteins, *Trends Biochem. Sci. 15*, 430−4.
51. Kelley, J. A., and Knight, K. L. (1997) Allosteric regulation of RecA protein function is mediated by Gln194, *J. Biol. Chem. 272*, 25778−82.
52. Zhou, Y., Morais-Cabral, J. H., Kaufman, A., and MacKinnon, R. (2001) Chemistry of ion coordination and hydration revealed by a K^+ channel-Fab complex at 2.0 Å resolution, *Nature 414*, 43−8.
53. Bourne, H. R., Sanders, D. A., and McCormick, F. (1991) The GTPase superfamily: Conserved structure and molecular mechanism, *Nature 349*, 117−27.
54. Voloshin, O. N., Wang, L., and Camerini-Otero, R. D. (2000) The homologous pairing domain of RecA also mediates the allosteric regulation of DNA binding and ATP hydrolysis: A remarkable concentration of functional residues, *J. Mol. Biol. 303*, 709−20.
55. Skiba, M. C., and Knight, K. L. (1994) Functionally important residues at a subunit interface site in the RecA protein from *Escherichia coli*, *J. Biol. Chem. 269*, 3823−8.
56. Kelley De Zutter, J., Forget, A. L., Logan, K. M., and Knight, K. L. (2001) Phe217 regulates the transfer of allosteric information across the subunit interface of the RecA protein filament, *Structure 9*, 47−55.
57. Wang, L., Voloshin, O. N., Stasiak, A., and Camerini-Otero, R. D. (1998) Homologous DNA pairing domain peptides of RecA protein: Intrinsic propensity to form β-structures and filaments, *J. Mol. Biol. 277*, 1−11.
58. Voloshin, O. N., Wang, L., and Camerini-Otero, R. D. (1996) Homologous DNA pairing promoted by a 20-amino acid peptide derived from RecA, *Science 272*, 868−72.
59. Hortnagel, K., Voloshin, O. N., Kinal, H. H., Ma, N., Schaffer-Judge, C., and Camerini-Otero, R. D. (1999) Saturation mutagenesis of the *E. coli* RecA loop L2 homologous DNA pairing region

reveals residues essential for recombination and recombinational repair, *J. Mol. Biol. 286*, 1097−106.
60. Cazaux, C., Blanchet, J. S., Dupuis, D., Villani, G., Defais, M., and Johnson, N. P. (1998) Investigation of the secondary DNA-binding site of the bacterial recombinase RecA, *J. Biol. Chem. 273*, 28799−804.
61. Mirshad, J. K., and Kowalczykowski, S. C. (2003) Biochemical characterization of a mutant RecA protein altered in DNA-binding loop 1, *Biochemistry 42*, 5945−54.
62. Morimatsu, K., and Horii, T. (1995) DNA-binding surface of RecA protein photochemical cross-linking of the first DNA binding site on RecA filament, *Eur. J. Biochem. 234*, 695−705.
63. Rehrauer, W. M., and Kowalczykowski, S. C. (1996) The DNA binding site(s) of the *Escherichia coli* RecA protein, *J. Biol. Chem. 271*, 11996−2002.
64. Wang, Y., and Adzuma, K. (1996) Differential proximity probing of two DNA binding sites in the *Escherichia coli* recA protein using photo-cross-linking methods, *Biochemistry 35*, 3563−71.
65. Namsaraev, E. A., and Berg, P. (1998) Binding of Rad51p to DNA. Interaction of Rad51p with single- and double-stranded DNA, *J. Biol. Chem. 273*, 6177−82.
66. Shan, Q., and Cox, M. M. (1997) RecA filament dynamics during DNA strand exchange reactions, *J. Biol. Chem. 272*, 11063−73.
67. Roca, A. I., and Singleton, S. F. (2003) Direct evaluation of a mechanism for activation of the RecA nucleoprotein filament, *J. Am. Chem. Soc. 125*, 15366−75.
68. Neuendorf, S. K., and Cox, M. M. (1986) Exchange of recA protein between adjacent recA protein-single-stranded DNA complexes, *J. Biol. Chem. 261*, 8276−82.
69. Menetski, J. P., and Kowalczykowski, S. C. (1987) Transfer of recA protein from one polynucleotide to another. Effect of ATP and determination of the processivity of ATP hydrolysis during transfer, *J. Biol. Chem. 262*, 2093−100.
70. Menetski, J. P., and Kowalczykowski, S. C. (1987) Transfer of recA protein from one polynucleotide to another. Kinetic evidence for a ternary intermediate during the transfer reaction, *J. Biol. Chem. 262*, 2085−92.
71. Kowalczykowski, S. C. (1991) Biochemistry of genetic recombination: Energetics and mechanism of DNA strand exchange, *Annu. Rev. Biophys. Biophys. Chem. 20*, 539−75.
72. Bugreev, D. V., and Mazin, A. V. (2004) Ca^{2+} activates human homologous recombination protein Rad51 by modulating its ATPase activity, *Proc. Natl. Acad. Sci. U.S.A. 101*, 9988−93.
73. Bugreev, D. V., Golub, E. I., Stasiak, A. Z., Stasiak, A., and Mazin, A. V. (2005) Activation of human meiosis-specific recombinase Dmc1 by Ca^{2+}, *J. Biol. Chem. 280*, 26886−95.
74. Shim, K. S., Schmutte, C., Tombline, G., Heinen, C. D., and Fishel, R. (2004) hXRCC2 enhances ADP/ATP processing and strand exchange by hRAD51, *J. Biol. Chem. 279*, 30385−94.

BI051222I